High endurance ferroelectric (La, Y) and (La, Gd) co-doped hafnium zirconate grown by atomic layer deposition.

Mihaela Ioana Popovici[1], Amey M. Walke[1], Jasper Bizindavyi[1], Johan Meersschaut[1], Kaustuv Banerjee[1], Goedele Potoms[1], Kostantine Katchko[1], Geert Van den Bosch[1], Romain Delhougne[1], Gouri Sankar Kar[1], Jan Van Houdt[1]*

[1]imec, Kapeldreef 75, 3001 Leuven, Belgium

KEYWORDS. Ferroelectrics, hafnium zirconate, doping, lanthanum, remnant polarization, endurance, coercive field.

ABSTRACT.

Thin films based on stoichiometric hafnium zirconate doped and co-doped with La, Gd and/or Y have been grown by atomic layer deposition on TiN electrodes. The resulting TiN-ferroelectric-TiN capacitors have shown high endurance up to 1E+11 switching cycles. The simultaneous use of two dopants (Y, La) or (Gd, La) in hafnium zirconate increases the amount of orthorhombic and tetragonal phases. Fatigue-free capacitors with remnant polarization ≥15 μC/cm^2 at 1E+11

endurance cycles have been obtained for dopants having an atomic fraction of about 1.2-1.8% and showing great promise as active materials for emerging memory applications.

INTRODUCTION

Oxides with a non-centrosymmetric fluorite structure have been extensively investigated in the last decade as potential ferroelectrics, since the appearance in 2011 of the first publication on ferroelectric Si doped HfO_2 [1]. However, a relatively high thermal budget is required to achieve ferroelectricity in Si doped HfO_2 [2,3]. A similar behavior has been found when HfO_2 was doped with smaller atoms, such as Al[4,5], or larger ones, such as Gd[6,7], Sr[8,9], Y[10,11] and La[12,13], which have enabled the stabilization of the ferroelectric phase in HfO_2 at low dopant concentrations (<10%). On the other hand, the addition of Zr reduces the needed thermal budget to below 600ºC[14]. Moreover, Zr has the ability to form a continuous solid solution with Hf[15], forming a mixed oxide $Hf_{1-x}Zr_xO_2$[16,17] which makes it a versatile candidate for ferroelectric semiconductor devices such as the ferroelectric random access memory (FERAM)[18-19] or ferroelectric field-effect transistor (FEFET)[20,21]. In the one transistor- one capacitor (1T-1C) FERAM device, data is stored in the form of the polarization state of the ferroelectric layer inside the metal-ferroelectric-metal (MFM) capacitor. The switch between two stable polarization states of the active ferroelectric material is achieved by reversing the direction of the applied electric field. To achieve a large memory window, a high remnant polarization ($2P_r$) of the ferroelectric oxide is required. Moreover, very high endurance, ≥1E+12 program-erase cycles is needed for RAM applications. The low voltages that are required (below 5 V) as well as the high writing speed[19] for FERAM make this a potentially attractive technology. A substantial increase in the amount of publications on ferroelectric $Hf_{1-x}Zr_xO_2$ MFM capacitors in the recent years by various research

groups[22,23-24] illustrates the interest in further investigation of doped hafnium zirconate for ferroelectric memories, with 1T-1C FERAM being one of the most promising candidates amongst the emerging memories due to its very low operating power consumption[18]. A low physical thickness of the films, below 15 nm, is easily achievable by atomic layer deposition (ALD)[25]. This method ensures very good uniformity and conformality control of deposition of the ferroelectric oxide and the metal electrodes in three-dimensional (3D) capacitors. Stoichiometric $Hf_{0.5}Zr_{0.5}O_2$ (referred to as HZO hereafter) grown by ALD requires a relatively low thermal budget (400-600ºC)[24,26,27] to achieve complete crystallization, which makes it a suitable candidate for back end of line applications[28]. It is believed that the ferroelectric behavior arises due to the formation of non-centrosymmetric orthorhombic Pca21 phase[29,30], where the oxygen ions are able to switch between two stable positions, which correspond to two stable polarization states [23]. The formation of orthorhombic HZO was evidenced by Muller et al.[14]. It has been found to be favored by the post-metallization anneal[31],[32] which induces sufficient strain[33] within the HZO to create favorable conditions for the growth of orthorhombic Pca21 with ferroelectric properties. Similar to HfO_2[7], the inclusion of dopants with a size larger or smaller than that of Hf and Zr ions, which are responsible for the distortion and internal stress within HZO, can have a beneficial effect on the ferroelectric properties, especially on the endurance[34]. A lower leakage current has been observed with La doping[35], allowing an improvement in the endurance of the ferroelectric oxide up to 1E+11 cycles[36]. This makes La doped HZO a good candidate for non-volatile memory applications[37]. However, a decrease in the remnant polarization with lanthanum dopant concentration has been observed at 1E+11 cycles[35]. Moreover, the beneficial effect of La doping on the endurance of polycrystalline HZO films[24] may be accompanied by a degradation of the retention, reducing the performance of the device[37].

Other dopants such as Y were also shown to induce ferroelectricity in HZO[38]. However, according to a thorough ab-initio study by Zhao et al[39] of different group III- dopants (which included La, Y , Al and Gd), La remains the most favorable dopant in terms of stabilizing the ferroelectric phase in HZO. Complementary doping with lanthanides or rare earth metals having smaller ionic radius than La^{3+} is expected to influence the lattice strain, the grain size, the relative ratio of the phases formed and furthermore the ferroelectric response of co-doped HZO. Reduction of monoclinic phase formation with the increase of tetragonal and cubic phases in a binary system of zirconia doped with trivalent Y^{3+}, Sr^{3+}, Yb^{3+} ions has been previously reported[40].Very low doping levels (less than ~1-2%) were shown to trigger remarkable responses in complex oxides such as the reduction of dielectric loss and inhibition of the grain growth[41,42]. Doping HZO with a combination of two dopants from the group III -dopants has not been investigated so far. In this paper we demonstrate that stoichiometric hafnium zirconate ($Hf_{0.5}Zr_{0.5}O_2$) co-doped with lanthanides and/or rare earth elements can induce fatigue-free endurance of at least 1E+11 cycles.

EXPERIMENTAL

In order to co - dope hafnium zirconate with two metals we employed two Pulsar reactor chambers connected to the same platform (ASM Microchemistry), which allowed depositions without air-break. Films with a thickness in the range of 9.5 nm to 12 nm were grown on 10 nm thick ALD TiN deposited on p++ doped 300 mm diameter Si wafers, by alternating HZO with the metallic dopant oxide (denoted here as X_2O_3, where X=Gd, La or Y) layers. In the first reactor, the growth of hafnium zirconate was performed at 300°C using $HfCl_4$ and $ZrCl_4$ as metal precursors and H_2O as oxidant. In the second reactor La_2O_3, Y_2O_3 or Gd_2O_3 were deposited using metalorganic precursors and H_2O as the oxidant. The La, Y and Gd dopant sources and suppliers were

$La(EtCp)_2(^iPr\text{-}AMD)$, $Y(^iPrCp)_3$ and $Gd(^iPrCp)_3$, respectively. The incorporation of La, Y and Gd dopants ($atoms/cm^2$) was monitored by Rutherford backscattering spectrometry (RBS) measurements[43]. The optimal metal dopant concentration for enhanced ferroelectric response (best remnant polarization-endurance trade-off) was found to be in the range of ~1 to 2 atomic percent (at.%), which is equivalent to about 3 ALD cycles of dopant oxide. In Figure 1a we show the Rutherford backscattering spectrum of a lanthanum-doped hafnium zirconate thin film deposited on a TiN bottom electrode on a silicon substrate, measured with a 3.02 MeV Helium ion beam. The signals corresponding to the various constituents are distinguished and allow one to quantify the concentrations and the thicknesses. Although the Zr:Hf ratio is close to one, the signal intensity of Zr is lower because of the lower scattering cross section. The concentration of lanthanum metal ions, La/(Hf+Zr+La), for this specific sample is 1.50 at%. The obtained concentration reflects the atomic ratio integrated over the layer and it is conceived that the dopant layer in the sample would be diffuse because of the localized roughness (0.5 nm) and near-surface diffusion during the deposition process (1 nm). The co-doped HZO films Figure 1 (b) were deposited following the general scheme of consecutive layers: $HZO/(X_2O_3/HZO)n/\ X_2O_3/HZO$, where n = 0, 1 or 2. For co-doping of HZO, two different X_2O_3 metal oxides were used, resulting in stacks such as $HZO/(La_2O_3/HZO)_2/Gd_2O_3/HZO$ or $HZO/\ La_2O_3/(HZO/Y_2O_3)_2/HZO$ for instance, by alternating the deposition of the component layers in the two reactors. For simplicity, the samples have been denoted as (2La, 1X):HZO, or (1La, 2X):HZO, where X can be either Gd or Y. For reference, single doped La:HZO, Y:HZO and Gd:HZO were deposited as well. A schematic of the stack is given in Figure 1 (c). The ferroelectric films were grown on 10 nm TiN bottom electrode. The top electrode (TE) consisted of 30 nm TiN which was deposited in a two-steps process. First, a 10 nm thick TiN layer was deposited, after which the stack was annealed at 550°C for 1 min in N_2. The

post-metallization anneal has the purpose to increase the amount of polar ferroelectric orthorhombic phase by mechanically confined crystallization as previously demonstrated in several studies[44,30]. Afterwards, an additional 20 nm thick TiN was deposited. All TiN layers were grown by atomic layer deposition at 450ºC using $TiCl_4$ and NH_3 as titanium and nitrogen sources. The patterning of TiN ensured the manufacturing of capacitors with a size of 80x60 μm^2 (Figure 1c).

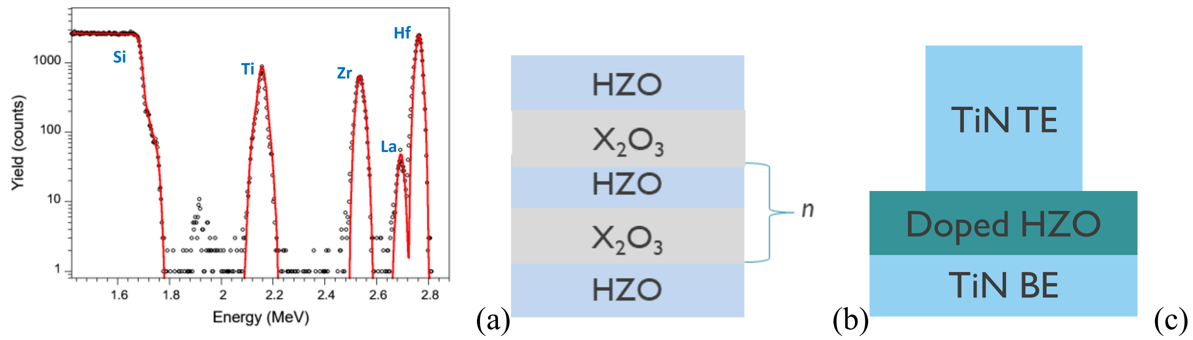

Figure 1. Rutherford backscattering spectrum obtained with a 3.020 MeV He+ primary ion beam on a lanthanum-doped hafnium-zirconate thin film deposited on TiN on a silicon substrate (a); Schematic of the HZO/(X_2O_3/HZO)n/ X_2O_3/HZO ferroelectric stack corresponding to doped HZO (b); TiN BE/Doped HZO ferroelectric/TiN TE capacitor (c). Here X is either La, Y or Gd.

Grazing incidence X-ray diffraction spectra (GIXRD) were acquired with Cu Kα radiation at 0.5º in a 2θ range between 20 and 65º. We quantified the relative amount of HZO phases present in the TiN–HZO–TiN capacitors by Rietveld refinement of the diffraction spectra performed with the Material Analysis Using Diffraction (Maud) software[45] in combination with crystallographic information files for monoclinic, orthorhombic, tetragonal, and cubic phases of ZrO_2 and cubic TiN following a model similar to the work of Park[46] and Mukundan[47]. The weighted profile R-factor (Rwp), which indicates the quality of the refinement, lies between 5.96-7.67%, while the

goodness of fit (σ) values varies between 0.99- 1.1. The error in phase quantification could amount up to ±8 % for the tetragonal phase, ±5 % for the orthorhombic phase, ±3 % for the cubic phase and ±1 % for the monoclinic phase.

All electrical measurements were performed on capacitors with a surface area of 4800 μm^2. The current and polarization (P) measurements as a function of electric field (E) were performed by applying bipolar triangular waveform voltage pulses with a frequency of 10 kHz. For endurance measurements, devices were cycled by applying bipolar fatigue pulses with a trapezoidal waveform where the rise, fall and flat time duration were of 200 ns each. Measurements to determine the electric breakdown field (E_{BD}) were performed on capacitors, pre-cycled up to 10^6 cycles at 3MV/cm, by applying a unipolar and unidirectional step voltage signal that increased from 0 V until breakdown (determined by observing a sharp increase in leakage current) with a voltage step increment of 100 mV and a step duration of 5 s (the measured current is averaged between 70% and 90% of the step duration).

RESULTS AND DISCUSSION

An initial series with 2, 3, 4 and 5 cycles Gd_2O_3 was used to grow ~12 nm thick Gd doped HZO (Gd:HZO) films. The ferroelectric films were completely crystallized as a result of the 550°C post-metallization anneal. The Gd:HZO layers contained the equivalent of 0.8 at. %, 1.3 at. %, 1.8 at. % and 2.4 at. % of Gd. Phase content was determined by Rietveld refinement of the GIXRD patterns (Figure 2a), which showed that gradual doping with Gd resulted in a decrease of monoclinic and orthorhombic phase content, while the tetragonal phase content strongly increased with more dopant cycles (Figure 2b).

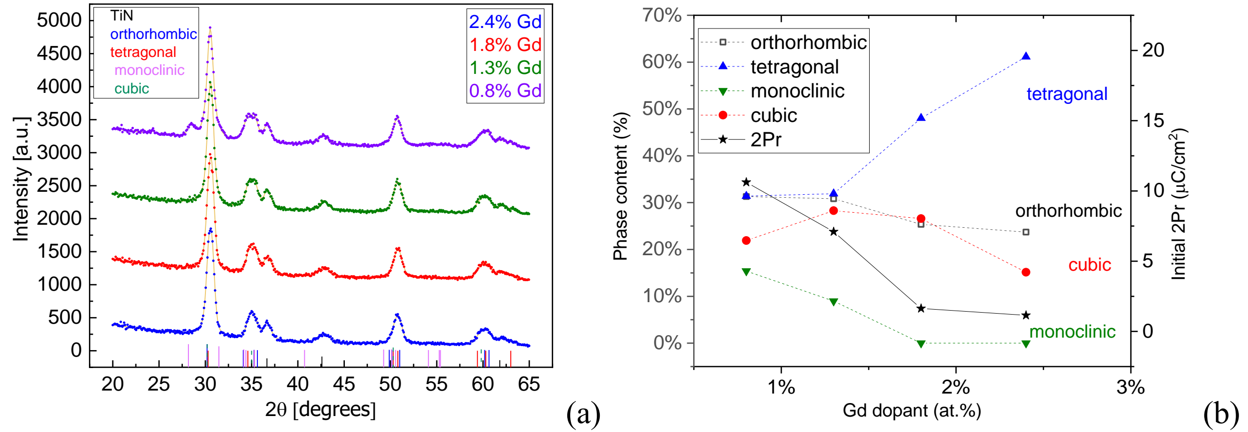

Figure 2. GIXRD patterns and data fit (beige line) (a) and computed phase content of ~12 nm Gd doped HZO as a function of the Gd concentration (at. %) and of the initial $2P_r$ (b).

P-E measurements up to 1E+7 cycles on multiple capacitors distributed over wafer area were shown in the Figure 3. In the case of the lowest Gd dopant concentrations (0.8 at. % and 1.3 at. %), a ferroelectric response with open hysteresis loops was clearly observed even for the initial switching cycles. The larger Gd dopant concentrations (1.8 and 2.4 at. %) resulted in pinched hysteresis loops, which could be due to the pinning of ferroelectric domains or to the presence of a predominantly antiferroelectric phase. The gradual opening of the hysteresis loops with increasing number of switching cycles, can be attributed to depinning of ferroelectric domains manifesting as wake-up behavior (Figure 3a). Larger values of the remnant polarization ($2P_r$) and coercive field ($2E_c$) were observed for HZO (Figure 3b) with a lower Gd dopant concentration. The trend was also maintained for a larger number of switching cycles with a maximum $2P_r$ of ~18 μC/cm^2 recorded at about 1E+6 cycles for 0.8 at. % Gd, while in the case of 1.3 at. % Gd a comparable maximal value of 14.5 μC/cm^2 was obtained at about 1E+7 cycles.

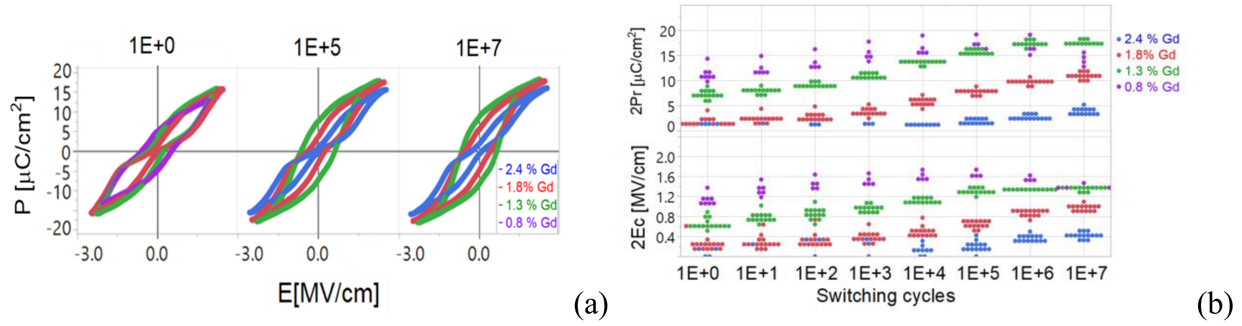

Figure 3. Polarization-electric field loops (a) and the extracted $2P_r$ and 2Ec vs. the number of switching cycles (b), as recorded for an applied electric field having a magnitude of 2.2 MV/cm as a function of Gd (at. %) content of ~ 12 nm thick films.

Based on the evolution of the extracted $2P_r$ with endurance cycling, the 1.3 at. % Gd doped HZO appeared to be the most promising layer in the series, as no fatigue was noted, unlike the case of 0.8 at. % Gd doped HZO containing the largest amount of non-ferroelectric monoclinic phase. The coexistence of monoclinic phase with orthorhombic ferroelectric one, has been previously associated with faster fatigue[24] and reduction of number of cycles until breakdown[48]. This behavior was seen in polycrystalline La doped Hf rich HZO[24] or La doped HfO_2[12] with randomly oriented grains as grown by ALD, which displayed a large initial remnant polarization and reduced wake-up effect. In contrast, Song et al showed that in the case of epitaxially grown HZO by pulse laser deposition[49], a positive effect on endurance was associated to monoclinic phase; one order of magnitude increase in endurance was observed when orthorhombic columnar grains were completely separated by monoclinic grains, however accompanied by a strong decrease in 2Pr below 2.5 μC/cm^2.

A dopant with ionic radius larger than that of Gd (namely La) and another one with radius smaller than that of Gd (namely Y) were also tried as co-dopants. To obtain the co-doping,

during the ALD growth one cycle of Gd_2O_3 deposition was substituted by one cycle of La_2O_3 deposition, and the stack was denoted (1La, 2Gd):HZO. A similar co-doped HZO with 1cycle of La_2O_3 and 2 cycles of Y_2O_3 was denoted (1La, 2Y):HZO. The phase content (Figure 4b) was also evaluated for the co-doped (1La, 2Gd):HZO and (1La, 2Y): HZO crystalline films, which displayed a similar GIXRD pattern to 3Gd:HZO (Figure 4a). The initial $2P_r$ was larger for (1La, 2Y):HZO, and reached a maximum remnant polarization of 17.7 μC/cm^2 at 3.2E+6 switching cycles while (1La, 2Gd):HZO and 3Gd:HZO had lower initial $2P_r$ values and somewhat delayed peak of maximum $2P_r$ was reached around 1E+7 switching cycles (Figure 4d).

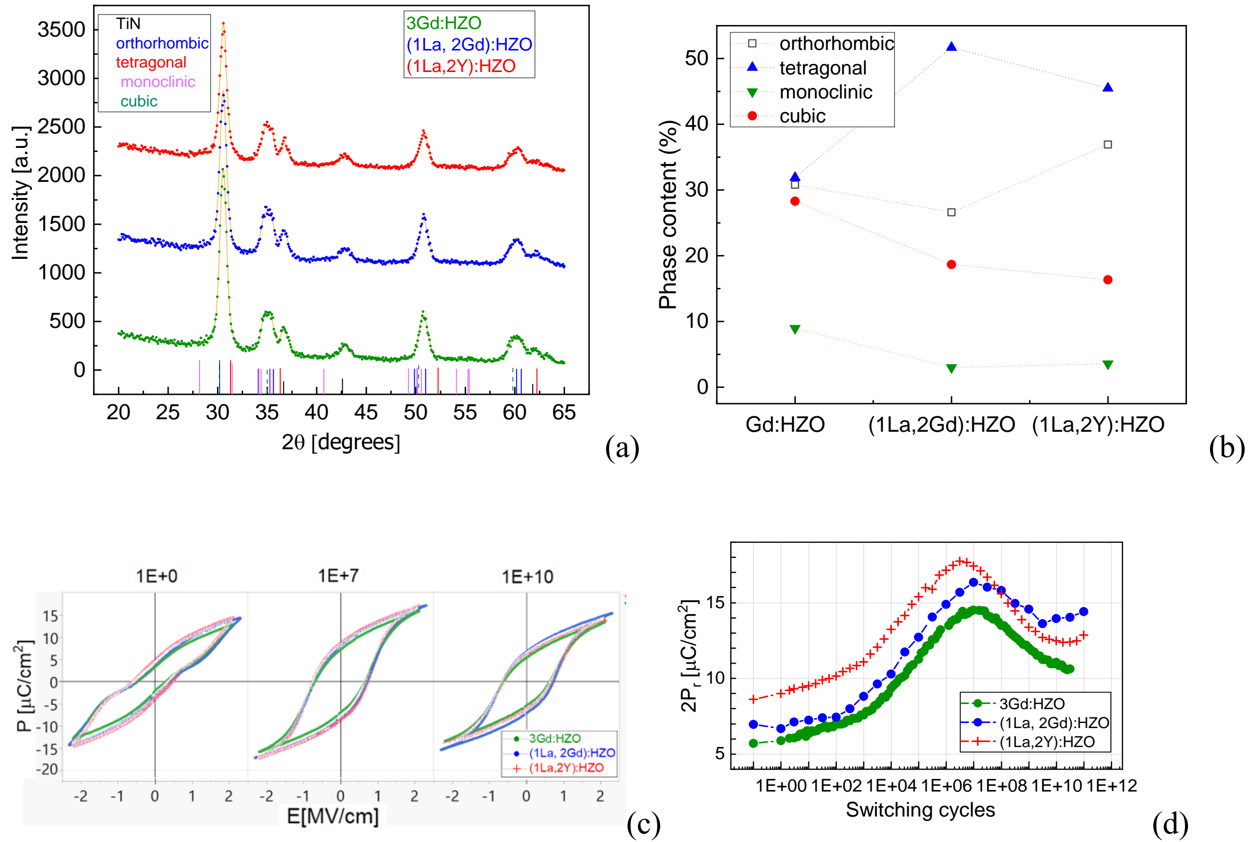

Figure 4. GIXRD pattern and data fit (beige line) (a), phase content extracted by Rietveld refinement (b), polarization-electric field loops (c) and $2P_r$ - switching cycles (d) for an applied electrical field magnitude of 2.2 MV/cm of ~12 nm thick films.

The orthorhombic content of the pristine samples was around 30 % for all three films, somewhat on the larger side for the case when Y co-dopant was present in concordance with the larger initial 2Pr. The pristine HZO films having (Gd, La) and (Y, La) as co-dopants showed a larger amount of tetragonal phase and a lower amount of cubic phase as compared to Gd doped HZO. Y is a rare earth metal whose Y^{3+} ion has a radius of 1.02 Å in the octahedral coordination. Gd and La belong to the lanthanide's family, with Gd having an ionic radius of 1.05Å and probably inducing a similar degree of distortion. The largest degree of lattice distortion is expected for the La dopant with a radius of 1.16 Å. A possible explanation for the larger amount of orthorhombic phase and consequently larger initial $2P_r$ in the case of co-doped (1La, 2Y):HZO is attributed to the large structural distortion which induces larger internal stress as a result of doping HZO with elements that have a large difference in radius. This hypothesis was confirmed by the increase in the total amount of tetragonal and orthorhombic phases, while the high symmetry cubic phase content was much reduced. A more remarkable decrease in monoclinic phase from ~9% in the case of 3Gd:HZO to ~3% for both (1La, 2Y) and (1La, 2Gd) co-doped HZO led to an improvement in the endurance. Lomenzo *et al.*[3] reported a similar behavior in mixed Al and Si doped HfO_2 and attributed a larger orthorhombic phase content to the increase in the in-plane tensile strain due to the smaller Al-doped HfO_2 lattice volume compared to the larger Si-doped HfO_2 lattice volume. The polarization - electric field measurements showed a peak in 2Pr that was achieved for all three samples around ~1E+6 – 1E+7 cycles followed by a decrease of polarization (Figure 4d). However, after 1E+9 cycles, the increase of polarization was again observed in the case of co-doped HZO films that have better endurance (1E+11 cycles) unlike 3Gd:HZO, which breaks down at 3.2E+10 cycles after reaching a $2P_r$ value of 10.6 μC/cm^2. Larger $2P_r$ values of 12.5 μC /cm^2 for (1La, 2Y):HZO and 14 μC/cm^2 for (1La, 2Gd):HZO were

obtained at 1E+11 switching cycles. The increase in $2P_r$ above 1+E10 switching cycles in the case of co-doped HZO could be attributed to a partial transition of the tetragonal phase into the orthorhombic phase as demonstrated through cycling in other studies on ferroelectric hafnium zirconate[50] or on ferroelectric Al and Si doped HfO_2[51]. The low energy barrier between the $P4_2/nmc$ tetragonal phase and the polar $Pca2_1$ orthorhombic phase is responsible for a spontaneous polarization observed in hafnia based systems[52]. Moreover in the case of ZrO_2 it was shown that the energy difference between the two phases amounts to only ~1 meV per formula unit[53], which makes the transition between the metastable tetragonal and the polar orthorhombic phase easier under applied electric-field pulses.

In a subsequent experiment, we scaled down the physical thickness of doped HZO from ~12nm to ~9.5 nm while keeping the same number of cycles of dopant. This resulted in slightly higher (~0.2 to 0.3 at. %) dopant concentration. Hereby, we demonstrate the effect of gradual substitution of La_2O_3 dopant cycles with Y_2O_3 dopant cycles for a total of 3 dopant cycles. The samples were denoted as 3La, (2La,1Y), (1Y, 2La) and 3Y doped HZO. Their GIXRD diffraction spectra were shown in Figure 5a. The phase deconvolution by Rietveld refinement was depicted in Figure 5b.

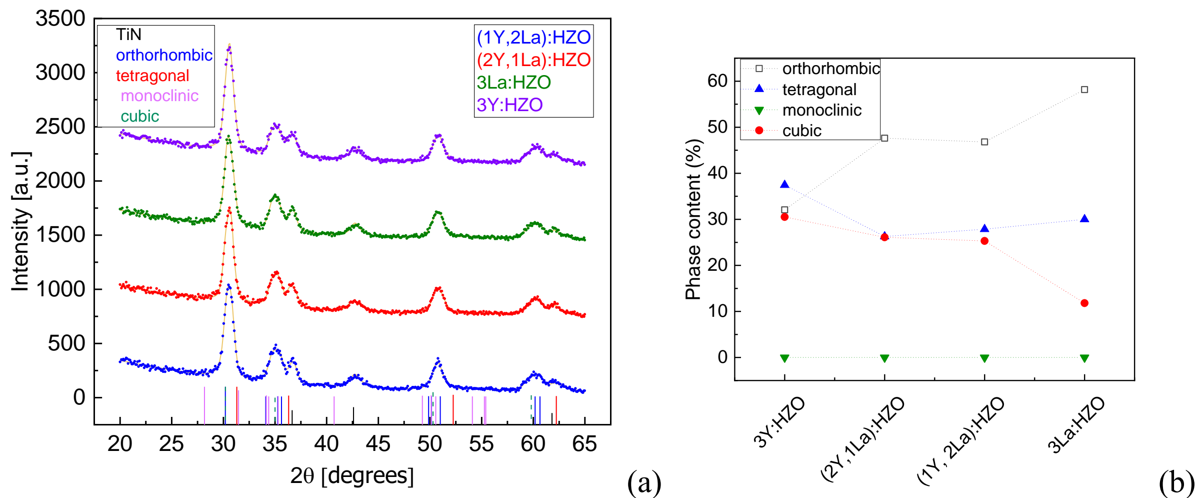

Figure 5. GIXRD patterns and data fit (beige line) (a) and the phase content of ~9.5 nm Y and La (co)-doped HZO (b).

A remarkable effect of downscaling the physical thickness was found to be the suppression of monoclinic phase formation, which was accompanied by an improved endurance. High endurance, up to 1E+10 cycles was previously reported in the case of 5 nm thick undoped HZO films [54]. In another study, bilayers of 5 nm antiferroelectric/5 nm ferroelectric HZO crystallized only into tetragonal and orthorhombic phase showed an improved endurance up to 1E+10 cycles that was attributed to further tetragonal - to - orthorhombic phase transition[55]. Generally, it is considered that presence of tetragonal phase favored by smaller grain size is a pre-requisite to form orthorhombic phase, whereas transition of orthorhombic to monoclinic phase is favored by a larger grain size[56]. Doping is another way to favor formation of tetragonal and orthorhombic phases over the monoclinic one, indicated by the absence of the characteristic (-111) and (111) monoclinic phase reflections expected at 2θ of ~28.5° and ~31.6°, respectively. This behavior was also observed by Kozodaev et al. in the case of La doped HZO films displaying high endurance up to 1E+11 cycles[36]. Doping with trivalent metals like La creates oxygen vacancies which favors formation of tetragonal and orthorhombic phases[34]. Repetitive external stimuli like electric field cycling lead eventually to increased conversion of tetragonal into orthorhombic phase[57].

In the case of our 9.5 nm Y and La doped and co-doped HZO films, the P-E measurements and the $2P_r$ extracted at different number of switching cycles were shown in the Figure 6. All four stacks survived 1E+11 cycles at a larger applied electric field magnitude of 2.5 MV/cm, which is in contrast to the results obtained for the 12 nm thick films that contained a small amount of monoclinic phase and required a lower applied electrical field magnitude of 2.2 MV/cm to

survive 1E+11 cycles. Nevertheless, strongly pinched hysteretic loops and a lower initial $2P_r$ for the 9.5 nm films as compared to the 12 nm films, were seen at the start of field cycling. The behavior is possibly related to an increase in domain pinning at a smaller grain size, which reduces the mobility of the domain walls[58]. Moreover, maintaining the same amount of trivalent dopant atoms (corresponding to 3 cycles ALD) and distributed in a smaller volume of hafnium zirconate in the case of thinner (9.5 nm) HZO films, possibly induces a higher density of oxygen vacancies that can be held responsible for a stronger internal bias field. During the electrical cycling the local density of oxygen decreases[59] and/or the oxygen vacancies rearrange in a more uniform manner[60] within the ferroelectric sandwiched between TiN electrodes[61, 62, 63] both previously associated to the wake-up effect. The initial $2P_r$ was found to decrease in the order La>2La+Y>2Y+La>Y (Figure 6). A larger initial orthorhombic phase content in the pristine state was observed for La doped HZO in comparison to (Y, La) co-doped HZO films, while 3Y:HZO showed the lowest orthorhombic phase content. For the Y containing HZO-based capacitors, the $2P_r$ was observed to gradually increase with cycling until ~1E+7 cycles, showing that a significant wake-up was required.

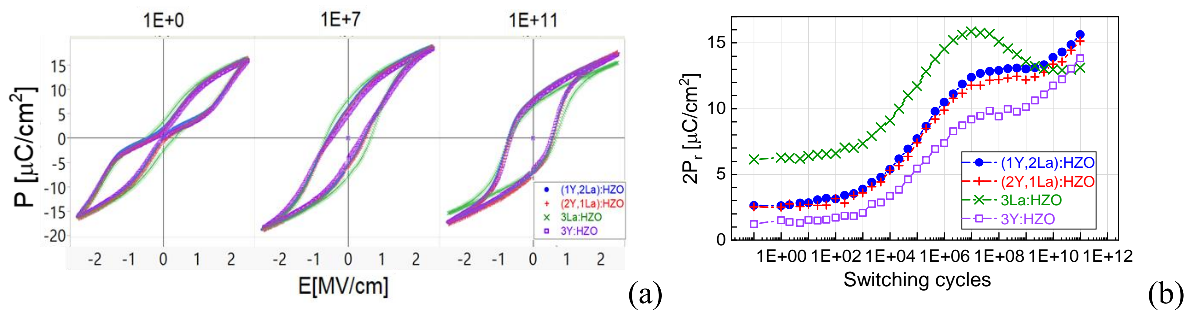

Figure 6. Polarization-electric field loops (a) and $2P_r$ as a function of switching cycles (b) of several ~9.5nm HZO layers doped and/or co-doped with Y and/or La, measured at an applied electric field magnitude of 2.5 MV/cm. On the other hand, a contribution to the prolonged wake-

up could also be related to the increased number of grains with o(111) orientation when HZO was doped with Y or (2Y, La) as compared to (1Y, 2La) co-doped HZO or La doped HZO. When La was incorporated into the HZO films, the signal of the peak at 2θ angle of ~35.0°, related to the contribution of o(002) oriented grains increased, while the peak corresponding to a 2θ angle of 30.5 ° related to the o(111) oriented grains decreased. Grains with an o(111) orientation are less well-aligned with the electric field direction than grains with the more preferred (002) orientation. Consequently, the increased preference of the grains in Y (co-)doped HZO films for the o(111) orientation correlates well with the lower initial $2P_r$ values measured for these films (Figure 6). Similar observations were made by Chernikova et al.[64] on La doped HZO grown on Ru, where a faster wake-up was observed when the grains favored an o(002) orientation.[65]To summarize, the prolonged wake-up observed in thinner (~9.5 nm) films up to ~1E+6 - 1E+7 cycles could be caused by a corroboration of several factors: a stronger pinning effects due to the larger amount of grain boundaries at smaller grain size [42,66], more grains containing unfavorable orientation of ferroelectric domains with gradual substitution of La by Y and a higher density of oxygen vacancies that requires more switching cycles for their redistribution. A completion of the wake-up stage is indicated by a plateau in 2Pr values between ~1E+7 and ~1E+9 cycles in the case of (Y, La) co-doped HZO and Y doped HZO. Beyond ~1E+9 cycles the remnant polarization increases again. This is likely the stage where the phase transition from tetragonal to orthorhombic phase starts taking place. An additional phase transition mechanism might happen in the case of La:HZO, unlike the (Y, La) co-doped HZO films or Y doped HZO. A shorter plateau with a maximum 2Pr of ~15.9 μC/cm^2 was observed for La:HZO, followed by a decrease of 2Pr which could be caused by the onset of orthorhombic to non-ferroelectric monoclinic phase transition[50] in the case of larger grains. Assuming a distribution of grain sizes in the 9.5 nm La:HZO films, this

phenomenon would be overlapping with the transition of some tetragonal into orthorhombic phase in the case of smaller grains and consequently 2Pr stabilized to ~ 13 μC/cm^2 . A decrease in 2Pr-switching cycles evolution was also observed for the 12 nm thick films, which due to lower dopant concentration and likely larger grains, were more prone to a faster transition from orthorhombic phase to non-ferroelectric monoclinic phase. The different growth rates of the dopant oxides and consequently, the different amount of dopant atomic content that is incorporated makes it difficult to compare La, Y and Gd at precisely the same thickness and atomic dopant concentration. However, it appears that in the 9.5-12 nm thickness range and for a 1.2-1.8 at. % dopant concentration a favorable window exists, in which either (Y, La) or (Gd, La) co-doped HZO show fatigue free behavior at ~ 2.2-2.5 MV/cm. The addition of Y reduced the coercive field compared to La (Figure 7), and the combination of the two showed improved $2P_r$ at 1 E+11 cycles (15.6 μC/cm^2 for (2La,Y) and 15.1 μC/cm^2 for (1La, 2Y) co-doped HZO capacitors.

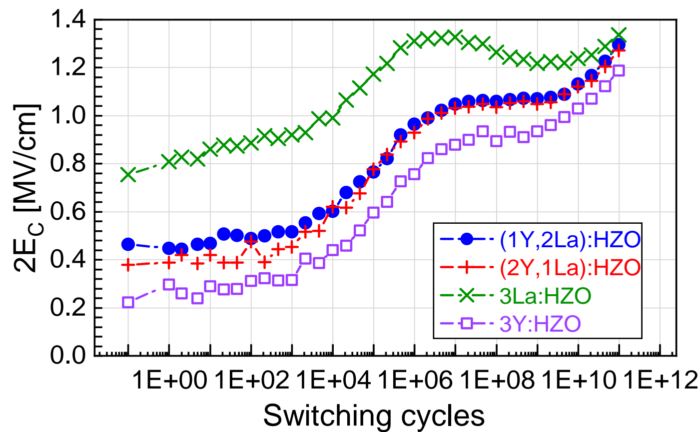

Figure 7. Evolution of coercive field 2Ec as a function of switching cycles of several ~9.5nm HZO layers doped and/or co-doped with Y and/or La, measured at an applied electric field magnitude of 2.5 MV/cm.

Reduction of 2Ec by adding a smaller (Y^{3+}) dopant is in agreement with previous observations regarding the effect of the dopant size on the coercive field of doped HfO_2[7]. Further, we have evaluated the breakdown field (E_{BD}) according to the procedure described in the Experimental section. It is considered that dielectric breakdown is due to the increase the leakage current and it corelates to the buildup of defects which eventually forms a conductive path[67]. For the ~9.5 nm thick films La doping led to larger E_{BD} (3.93 MV/cm) as compared to Y doping (3.75 MV/cm), while (Y, La) co-doped HZO showed an intermediate behavior. (2La, Y) co-doped HZO showed an E_{BD} of 3.87 MV/cm for a thickness of 9.5 nm. E_{BD} decreased to 3.16 MV/cm in the case of thicker (~12 nm) films. Lower E_{BD} for thicker film is likely related to the presence of monoclinic phase (~3%) in agreement with Böscke et al that reported monoclinic phase presence led to local defects and increased the leakage current[68]. Further cycling is required to assess if co-doped HZO films can withstand even larger numbers of switching cycles. The $2P_r$ at 1E+11 cycles for 3La:HZO is lower in comparison to the work of Kozodaev et al[36] at comparable La doping level. This is likely caused by the precursor/oxidant selection[69,70], which induces particular nucleation/growth conditions[71] of the HZO in combination with the annealing conditions[72], and the electrodes[64, 72-73] that are employed. Therefore, both the intrinsic stress related to the doped HZO grain growth and the mechanical stress induced by the TiN electrodes, their thickness, the deposition conditions, and the Ti/N ratio all have an impact on the remnant polarization. Our results confirm nonetheless the fact that La is the most favorable dopant in terms of stabilizing the ferroelectric phase in HZO as also shown by Zhao et al through their ab-initio simulations[39]. Moreover, the co-doping of the HZO improves the endurance and reduces the coercive field. Depending on the required application, it is also possible to control by optimizing the La, Gd and/or Y co-doping concentration at least one or more of the following parameters: remnant

polarization, coercive field, endurance, fatigue, retention, and the wake-up behavior in the co-doped HZO layer as desired.

Conclusions

We have demonstrated for the first time that a combination of two dopants can result in high endurance (1E+11 switching cycles) and fatigue-free HZO films. Besides La, both Y and Gd have been found to have a potentially beneficial role in improving the endurance up to or beyond 1+E11 switching cycles and to favor the (partial) transition of tetragonal into orthorhombic phase, which is likely the cause of the gradual increase in $2P_r$ observed beyond ~1E+10 cycles. The presence of two dopants induces a larger structural distortion within hafnium zirconate based on the differences in ionic radius between both dopants. The resulted increase in intrinsic stress modulates the relative tetragonal/orthorhombic phase content, and it is beneficial for the reduction in the amount of the high symmetry phases such as the cubic phase and for the suppression of the monoclinic phase formation below 10 nm.

AUTHOR INFORMATION

Corresponding Author

*Mihaela Ioana Popovici, imec, Kapeldreef 75, 3001 Leuven, Belgium.

https://orcid.org/**0000-0002-9838-1088**

email: Mihaela.Ioana.Popovici@imec.be.

Author Contributions

The manuscript was written through contributions of all authors. All authors have given approval to the final version of the manuscript.

Notes

The authors declare no competing financial interest.

ACKNOWLEDGMENT

This work is performed under imec's industrial affiliation program on ferroelectrics.

ABBREVIATIONS

HZO, $Hf_{0.5}Zr_{0.5}O_2$, stoichiometric hafnium zirconate; GIXRD, grazing incidence X-ray diffraction, RBS, Rutherford backscattering spectrometry; $2P_r$, remnant polarization; 2Ec, coercive field; P-polarization, E-applied electric field; E_{BD}, electric breakdown field.

REFERENCES

(1) Böscke, T. S.; Müller, J.; Bräuhaus, D.; Schröder, U.; Böttger, U. Ferroelectricity in Hafnium Oxide Thin Films. *Appl. Phys. Lett.* **2011**, *99* (10), 102903.

(2) Lomenzo, P. D.; Zhao, P.; Takmeel, Q.; Moghaddam, S.; Nishida, T.; Nelson, M.; Fancher, C. M.; Grimley, E. D.; Sang, X.; LeBeau, J. M.; Jones, J. L. Ferroelectric Phenomena in Si-Doped HfO_2 Thin Films with TiN and Ir Electrodes. *J. Vac. Sci. Technol. B Nanotechnol. Microelectron. Mater. Process. Meas. Phenom.* **2014**, *32* (3), 03D123.

(3) Lomenzo, P. D.; Takmeel, Q.; Zhou, C.; Chung, C.-C.; Moghaddam, S.; Jones, J. L.; Nishida, T. Mixed Al and Si Doping in Ferroelectric HfO_2 Thin Films. *Appl. Phys. Lett.* **2015**, *107* (24), 242903.

(4) Florent, K.; Lavizzari, S.; Popovici, M.; Di Piazza, L.; Celano, U.; Groeseneken, G.; Van Houdt, J. Understanding Ferroelectric Al:HfO $_2$ Thin Films with Si-Based Electrodes for 3D Applications. *J. Appl. Phys.* **2017**, *121* (20), 204103.

(5) Liu, X.; Yao, L.; Cheng, Y.; Xiao, B. High Annealing Temperature Assisted Broadening of the Ferroelectric Concentration Window in Al:HfO_2 MFS Structures. *Jpn. J. Appl. Phys.* **2019**, *58* (9), 090903.

(6) Adelmann, C.; Schram, T.; Chew, S.-A.; Woicik, J. C.; Brizzi, S.; Tallarida, M.; Schmeisser, D.; Horiguchi, N.; Van Elshocht, S.; Ragnarsson, L.-Å. On the Scalability of Doped Hafnia Thin Films. *Appl. Phys. Lett.* **2014**, *104* (12), 122906..

(7) Schroeder, U.; Yurchuk, E.; Müller, J.; Martin, D.; Schenk, T.; Polakowski, P.; Adelmann, C.; Popovici, M. I.; Kalinin, S. V.; Mikolajick, T. Impact of Different Dopants on the Switching Properties of Ferroelectric Hafniumoxide. *Jpn. J. Appl. Phys.* **2014**, *53* (8S1), 08LE02.

(8) Schenk, T.; Schroeder, U.; Pešić, M.; Popovici, M.; Pershin, Y. V.; Mikolajick, T. Electric Field Cycling Behavior of Ferroelectric Hafnium Oxide. *ACS Appl. Mater. Interfaces* **2014**, *6* (22), 19744–19751.

(9) Park, M. H.; Lee, Y. H.; Hwang, C. S. Understanding Ferroelectric Phase Formation in Doped HfO_2 Thin Films Based on Classical Nucleation Theory. *Nanoscale* **2019**, *11* (41), 19477–19487.
(10) Tashiro, Y.; Shimizu, T.; Mimura, T.; Funakubo, H. Comprehensive Study on the Kinetic Formation of the Orthorhombic Ferroelectric Phase in Epitaxial Y-Doped Ferroelectric HfO_2 Thin Films. *ACS Appl. Electron. Mater.* **2021**, *3* (7), 3123–3130.
(11) Mimura, T.; Shimizu, T.; Uchida, H.; Sakata, O.; Funakubo, H. Thickness-Dependent Crystal Structure and Electric Properties of Epitaxial Ferroelectric Y_2O_3 -HfO_2 Films. *Appl. Phys. Lett.* **2018**, *113* (10), 102901.
(12) Schroeder, U.; Richter, C.; Park, M. H.; Schenk, T.; Pešić, M.; Hoffmann, M.; Fengler, F. P. G.; Pohl, D.; Rellinghaus, B.; Zhou, C.; Chung, C.-C.; Jones, J. L.; Mikolajick, T. Lanthanum-Doped Hafnium Oxide: A Robust Ferroelectric Material. *Inorg. Chem.* **2018**, *57* (5), 2752–2765.
(13) Chernikova, A. G.; Kuzmichev, D. S.; Negrov, D. V.; Kozodaev, M. G.; Polyakov, S. N.; Markeev, A. M. Ferroelectric Properties of Full Plasma-Enhanced ALD TiN/La:HfO_2 /TiN Stacks. *Appl. Phys. Lett.* **2016**, *108* (24), 242905.
(14) Müller, J.; Böscke, T. S.; Bräuhaus, D.; Schröder, U.; Böttger, U.; Sundqvist, J.; Kücher, P.; Mikolajick, T.; Frey, L. Ferroelectric $Zr_{0.5}Hf_{0.5}O_2$ Thin Films for Nonvolatile Memory Applications. *Appl. Phys. Lett.* **2011**, *99* (11), 112901.
(15) Müller, J.; Böscke, T. S.; Schröder, U.; Mueller, S.; Bräuhaus, D.; Böttger, U.; Frey, L.; Mikolajick, T. Ferroelectricity in Simple Binary ZrO2 and HfO2. *Nano Lett.* **2012**, *12* (8), 4318–4323.
(16) Mittmann, T.; Fengler, F. P. G.; Richter, C.; Park, M. H.; Mikolajick, T.; Schroeder, U. Optimizing Process Conditions for Improved Hf1−xZrxO2 Ferroelectric Capacitor Performance. *Microelectron. Eng.* **2017**, *178*, 48–51.
(17) Hsain, H. A.; Lee, Y.; Parsons, G.; Jones, J. L. Compositional Dependence of Crystallization Temperatures and Phase Evolution in Hafnia-Zirconia $(Hf_xZr_{1-x})O_2$ Thin Films. *Appl. Phys. Lett.* **2020**, *116* (19), 192901.
(18) Cao, Q.; Lü, W.; Wang, X. R.; Guan, X.; Wang, L.; Yan, S.; Wu, T.; Wang, X. Nonvolatile Multistates Memories for High-Density Data Storage. *ACS Appl. Mater. Interfaces* **2020**, *12* (38), 42449–42471.
(19) Okuno, J.; Kunihiro, T.; Konishi, K.; Maemura, H.; Shuto, Y.; Sugaya, F.; Materano, M.; Ali, T.; Lederer, M.; Kuehnel, K.; Seidel, K.; Schroeder, U.; Mikolajick, T.; Tsukamoto, M.; Umebayashi, T. High-Endurance and Low-Voltage Operation of 1T1C FeRAM Arrays for Nonvolatile Memory Application. In *2021 IEEE International Memory Workshop (IMW)*; IEEE: Dresden, Germany, 2021; pp 1–3. https://doi.org/10.1109/IMW51353.2021.9439595.
(20) Chen, K.-T.; Chen, H.-Y.; Liao, C.-Y.; Siang, G.-Y.; Lo, C.; Liao, M.-H.; Li, K.-S.; Chang, S. T.; Lee, M. H. Non-Volatile Ferroelectric FETs Using 5-Nm Hf $_{0.5}$ Zr $_{0.5}$ O $_2$ With High Data Retention and Read Endurance for 1T Memory Applications. *IEEE Electron Device Lett.* **2019**, *40* (3), 399–402. https://doi.org/10.1109/LED.2019.2896231.
(21) Zeng, B.; Liao, M.; Peng, Q.; Xiao, W.; Liao, J.; Zheng, S.; Zhou, Y. 2-Bit/Cell Operation of Hf $_{0.5}$ Zr $_{0.5}$ O $_2$ Based FeFET Memory Devices for NAND Applications. *IEEE J. Electron Devices Soc.* **2019**, *7*, 551–556. https://doi.org/10.1109/JEDS.2019.2913426.
(22) Kim, S. J.; Mohan, J.; Summerfelt, S. R.; Kim, J. Ferroelectric Hf0.5Zr0.5O2 Thin Films: A Review of Recent Advances. *JOM* **2019**, *71* (1), 246–255. https://doi.org/10.1007/s11837-018-3140-5.

(23) Mikolajick, T.; Schroeder, U.; Slesazeck, S. The Past, the Present, and the Future of Ferroelectric Memories. *IEEE Trans. Electron Devices* **2020**, *67* (4), 1434–1443. https://doi.org/10.1109/TED.2020.2976148.
(24) Popovici, M.; Walke, A. M.; Banerjee, K.; Ronchi, N.; Meersschaut, J.; Celano, U.; McMitchell, S.; Spampinato, V.; Franquet, A.; Favia, P.; Swerts, J.; Van den Bosch, G.; Van Houdt, J. Ferroelectric La-Doped ZrO2/HfxZr1−xO2 Bilayer Stacks with Enhanced Endurance. *Phys. Status Solidi RRL – Rapid Res. Lett.* **2021**, *15* (5), 2100033.
(25) Lee, H.; Choe, D.-H.; Jo, S.; Kim, J.-H.; Lee, H. H.; Shin, H.-J.; Park, Y.; Kang, S.; Cho, Y.; Park, S.; Moon, T.; Eom, D.; Leem, M.; Kim, Y.; Heo, J.; Lee, E.; Kim, H. Unveiling the Origin of Robust Ferroelectricity in Sub-2 Nm Hafnium Zirconium Oxide Films. *ACS Appl. Mater. Interfaces* **2021**, *13* (30), 36499–36506.
(26) Kim, S. J.; Mohan, J.; Kim, H. S.; Lee, J.; Hwang, S. M.; Narayan, D.; Lee, J.-G.; Young, C. D.; Colombo, L.; Goodman, G.; Wan, A. S.; Cha, P.-R.; Summerfelt, S. R.; San, T.; Kim, J. Effect of Hydrogen Derived from Oxygen Source on Low-Temperature Ferroelectric TiN/$Hf_{0.5}Zr_{0.5}O_2$/TiN Capacitors. *Appl. Phys. Lett.* **2019**, *115* (18), 182901.
(27) Chang, S.-J.; Teng, C.-Y.; Lin, Y.-J.; Wu, T.-M.; Lee, M.-H.; Lin, B.-H.; Tang, M.-T.; Wu, T.-S.; Hu, C.; Tang, Ethan. Y.-T.; Tseng, Y.-C. Visualizing Ferroelectric Uniformity of $Hf_{1-x}Zr_xO_2$ Films Using X-Ray Mapping. *ACS Appl. Mater. Interfaces* **2021**, *13* (24), 29212–29221.
(28) Hur, J.; Luo, Y.-C.; Tasneem, N.; Khan, A. I.; Yu, S. Ferroelectric Hafnium Zirconium Oxide Compatible With Back-End-of-Line Process. *IEEE Trans. Electron Devices* **2021**, *68* (7), 3176–3180. https://doi.org/10.1109/TED.2021.3072610.
(29) Lowther, J. E.; Dewhurst, J. K.; Leger, J. M.; Haines, J. Relative Stability of ZrO 2 and HfO 2 Structural Phases. *Phys. Rev. B* **1999**, *60* (21), 14485–14488.
(30) Park, M. H.; Lee, Y. H.; Kim, H. J.; Kim, Y. J.; Moon, T.; Kim, K. D.; Müller, J.; Kersch, A.; Schroeder, U.; Mikolajick, T.; Hwang, C. S. Ferroelectricity and Antiferroelectricity of Doped Thin HfO_2-Based Films. *Adv. Mater.* **2015**, *27* (11), 1811–1831.
(31) Lee, Y.; Alex Hsain, H.; Fields, S. S.; Jaszewski, S. T.; Horgan, M. D.; Edgington, P. G.; Ihlefeld, J. F.; Parsons, G. N.; Jones, J. L. Unexpectedly Large Remanent Polarization of $Hf_{0.5}Zr_{0.5}O_2$ Metal–Ferroelectric–Metal Capacitor Fabricated without Breaking Vacuum. *Appl. Phys. Lett.* **2021**, *118* (1), 012903.
(32) O'Connor, É.; Halter, M.; Eltes, F.; Sousa, M.; Kellock, A.; Abel, S.; Fompeyrine, J. Stabilization of Ferroelectric $Hf_xZr_{1-x}O_2$ Films Using a Millisecond Flash Lamp Annealing Technique. *APL Mater.* **2018**, *6* (12), 121103.
(33) Batra, R.; Tran, H. D.; Ramprasad, R. Stabilization of Metastable Phases in Hafnia Owing to Surface Energy Effects. *Appl. Phys. Lett.* **2016**, *108* (17), 172902.
(34) Mehmood, F.; Mikolajick, T.; Schroeder, U. Lanthanum Doping Induced Structural Changes and Their Implications on Ferroelectric Properties of $Hf_{1-x}Zr_xO_2$ Thin Film. *Appl. Phys. Lett.* **2020**, *117* (9), 092902.
(35) Chernikova, A. G.; Kozodaev, M. G.; Negrov, D. V.; Korostylev, E. V.; Park, M. H.; Schroeder, U.; Hwang, C. S.; Markeev, A. M. Improved Ferroelectric Switching Endurance of La-Doped $Hf_{0.5}Zr_{0.5}O_2$ Thin Films. *ACS Appl. Mater. Interfaces* **2018**, *10* (3), 2701–2708.
(36) Kozodaev, M. G.; Chernikova, A. G.; Korostylev, E. V.; Park, M. H.; Khakimov, R. R.; Hwang, C. S.; Markeev, A. M. Mitigating Wakeup Effect and Improving Endurance of

Ferroelectric HfO_2-ZrO_2 Thin Films by Careful La-Doping. *J. Appl. Phys.* **2019**, *125* (3), 034101.
(37) Mehmood, F.; Hoffmann, M.; Lomenzo, P. D.; Richter, C.; Materano, M.; Mikolajick, T.; Schroeder, U. Bulk Depolarization Fields as a Major Contributor to the Ferroelectric Reliability Performance in Lanthanum Doped $Hf_{0.5}Zr_{0.5}O_2$ Capacitors. *Adv. Mater. Interfaces* **2019**, *6* (21), 1901180.
(38) Mohit; Haga, K.; Tokumitsu, E. Electrical Properties of Yttrium-Doped Hafnium-Zirconium Dioxide Thin Films Prepared by Solution Process for Ferroelectric Gate Insulator TFT Application. *Jpn. J. Appl. Phys.* **2020**, *59* (SM), SMMB02.
(39) Zhao, L.; Liu, J.; Zhao, Y. Systematic Studies of the Effects of Group-III Dopants (La, Y, Al, and Gd) in $Hf_{0.5}Zr_{0.5}O_2$ Ferroelectrics by *Ab Initio* Simulations. *Appl. Phys. Lett.* **2021**, *119* (17), 172903.
(40) Jiang, S. L.; Huang, X.; He, Z. Phase Transformation and Lattice Parameter Changes of Trivalent Rare Earth Doped YSZ as a Function of Temperature. *J. Mater. Eng. Perform.* **2016**, *25* (11), 4686–4694.
(41) Xu, Z.; Qiang, H.; Chen, Y.; Chen, Z. Microstructure and Enhanced Dielectric Properties of Yttrium and Zirconium Co-Doped CaCu3Ti4O12 Ceramics. *Mater. Chem. Phys.* **2017**, *191*, 1–5.
(42) Cao, H.; Zheng, H.; Fan, L.; Cheng, Z.; Zhou, J.; Wu, Q.; Zheng, P.; Zheng, L.; Zhang, Y. Structural, Morphological, Dielectric and Magnetic Properties of Zn-Zr Co-doping Yttrium Iron Garnet. *Int. J. Appl. Ceram. Technol.* **2020**, *17* (2), 813–822..
(43) Meersschaut, J.; Vandervorst, W. High-Throughput Ion Beam Analysis at Imec. *Nucl. Instrum. Methods Phys. Res. Sect. B Beam Interact. Mater. At.* **2017**, *406*, 25–29.
(44) Müller, J.; Schröder, U.; Böscke, T. S.; Müller, I.; Böttger, U.; Wilde, L.; Sundqvist, J.; Lemberger, M.; Kücher, P.; Mikolajick, T.; Frey, L. Ferroelectricity in Yttrium-Doped Hafnium Oxide. *J. Appl. Phys.* **2011**, *110* (11), 114113.
(45) Lutterotti, L. Total Pattern Fitting for the Combined Size–Strain–Stress–Texture Determination in Thin Film Diffraction. *Nucl. Instrum. Methods Phys. Res. Sect. B Beam Interact. Mater. At.* **2010**, *268* (3–4), 334–340.
(46) Park, M. H.; Schenk, T.; Fancher, C. M.; Grimley, E. D.; Zhou, C.; Richter, C.; LeBeau, J. M.; Jones, J. L.; Mikolajick, T.; Schroeder, U. A Comprehensive Study on the Structural Evolution of HfO_2 Thin Films Doped with Various Dopants. *J. Mater. Chem. C* **2017**, *5* (19), 4677–4690.
(47) Mukundan, V.; Consiglio, S.; Triyoso, D. H.; Tapily, K.; Schujman, S.; Mart, C.; Kämpfe, T.; Weinreich, W.; Jordan-Sweet, J.; Clark, R. D.; Leusink, G. J.; Diebold, A. C. Quantifying Non-Centrosymmetric Orthorhombic Phase Fraction in 10 Nm Ferroelectric $Hf_{0.5}Zr_{0.5}O_2$ Films. *Appl. Phys. Lett.* **2020**, *117* (26), 262905.
(48) Mittmann, T.; Fengler, F. P. G.; Richter, C.; Park, M. H.; Mikolajick, T.; Schroeder, U. Optimizing Process Conditions for Improved Hf1−xZrxO2 Ferroelectric Capacitor Performance. *Microelectron. Eng.* **2017**, *178*, 48–51.
(49) Song, T.; Estandía, S.; Tan, H.; Dix, N.; Gàzquez, J.; Fina, I.; Sánchez, F. Positive Effect of Parasitic Monoclinic Phase of $Hf_{0.5}Zr_{0.5}O_2$ on Ferroelectric Endurance. *Adv. Electron. Mater.* **2022**, *8* (1), 2100420.
(50) Fields, S. S.; Smith, S. W.; Ryan, P. J.; Jaszewski, S. T.; Brummel, I. A.; Salanova, A.; Esteves, G.; Wolfley, S. L.; Henry, M. D.; Davids, P. S.; Ihlefeld, J. F. Phase-Exchange-

Driven Wake-Up and Fatigue in Ferroelectric Hafnium Zirconium Oxide Films. *ACS Appl. Mater. Interfaces* **2020**, *12* (23), 26577–26585.
(51) McMitchell, S. R. C.; Clima, S.; Ronchi, N.; Banerjee, K.; Celano, U.; Popovici, M.; Di Piazza, L.; Van den Bosch, G.; Van Houdt, J. Elucidating Possible Crystallographic Origins of Wake-up Mechanisms in Ferroelectric Hafnia. *Appl. Phys. Lett.* **2021**, *118* (9), 092902.
(52) Huan, T. D.; Sharma, V.; Rossetti, G. A.; Ramprasad, R. Pathways towards Ferroelectricity in Hafnia. *Phys. Rev. B* **2014**, *90* (6), 064111. https://doi.org/10.1103/PhysRevB.90.064111.
(53) Reyes-Lillo, S. E.; Garrity, K. F.; Rabe, K. M. Antiferroelectricity in Thin-Film ZrO2 from First Principles. *Phys. Rev. B* **2014**, *90* (14), 140103.
(54) Kim, S. J.; Mohan, J.; Kim, H. S.; Lee, J.; Young, C. D.; Colombo, L.; Summerfelt, S. R.; San, T.; Kim, J. Low-Voltage Operation and High Endurance of 5-Nm Ferroelectric $Hf_{0.5}Zr_{0.5}O_2$ Capacitors. *Appl. Phys. Lett.* **2018**, *113* (18), 182903.
(55) Lo, C.; Chen, C.-K.; Chang, C.-F.; Zhang, F.-S.; Lu, Z.-H.; Chao, T.-S. High Endurance and Low Fatigue Effect of Bilayer Stacked Antiferroelectric/Ferroelectric $Hf_xZr_{1-x}O_2$. *IEEE Electron Device Lett.* **2022**, *43* (2), 224–227..
(56) Park, M. H.; Schenk, T.; Fancher, C. M.; Grimley, E. D.; Zhou, C.; Richter, C.; LeBeau, J. M.; Jones, J. L.; Mikolajick, T.; Schroeder, U. A Comprehensive Study on the Structural Evolution of HfO_2 Thin Films Doped with Various Dopants. *J. Mater. Chem. C* **2017**, *5* (19), 4677–4690.
(57) Tashiro, Y.; Shimizu, T.; Mimura, T.; Funakubo, H. Comprehensive Study on the Kinetic Formation of the Orthorhombic Ferroelectric Phase in Epitaxial Y-Doped Ferroelectric HfO_2 Thin Films. *ACS Appl. Electron. Mater.* **2021**, *3* (7), 3123–3130.
(58) Yan, F.; Bao, P.; Chan, H. L. W.; Choy, C.-L.; Wang, Y. The Grain Size Effect of Pb(Zr0.3Ti0.7)O3 Thin Films. *Thin Solid Films* **2002**, *406* (1–2), 282–285.
(59) Chouprik, A.; Spiridonov, M.; Zarubin, S.; Kirtaev, R.; Mikheev, V.; Lebedinskii, Y.; Zakharchenko, S.; Negrov, D. Wake-Up in a $Hf_{0.5}Zr_{0.5}O_2$ Film: A Cycle-by-Cycle Emergence of the Remnant Polarization via the Domain Depinning and the Vanishing of the Anomalous Polarization Switching. *ACS Appl. Electron. Mater.* **2019**, *1* (3), 275–287.
(60) Pešić, M.; Fengler, F. P. G.; Larcher, L.; Padovani, A.; Schenk, T.; Grimley, E. D.; Sang, X.; LeBeau, J. M.; Slesazeck, S.; Schroeder, U.; Mikolajick, T. Physical Mechanisms behind the Field-Cycling Behavior of HfO_2 -Based Ferroelectric Capacitors. *Adv. Funct. Mater.* **2016**, *26* (25), 4601–4612.
(61) Hamouda, W.; Pancotti, A.; Lubin, C.; Tortech, L.; Richter, C.; Mikolajick, T.; Schroeder, U.; Barrett, N. Physical Chemistry of the TiN/$Hf_{0.5}Zr_{0.5}O_2$ Interface. *J. Appl. Phys.* **2020**, *127* (6), 064105.
(62) Park, M. H.; Lee, Y. H.; Mikolajick, T.; Schroeder, U.; Hwang, C. S. Review and Perspective on Ferroelectric HfO2-Based Thin Films for Memory Applications. *MRS Commun.* **2018**, *8* (3), 795–808.
(63) Walke, A. M.; Popovici, M. I.; Banerjee, K.; Clima, S.; Kumbhare, P., Hoflijk, I.; Conard, T.; Van den Bosch, G; Delhougne, R; Sankar Kar, G; Van Houdt, J. Electrical Investigation of Wake-up in High Endurance Fatigue-Free La and Y Doped HZO Metal-Ferroelectric-Metal Capacitors. submitted to *IEEE Transactions on Electron Devices*.

(64) Chernikova, A. G.; Kozodaev, M. G.; Khakimov, R. R.; Polyakov, S. N.; Markeev, A. M. Influence of ALD Ru Bottom Electrode on Ferroelectric Properties of $Hf_{0.5}Zr_{0.5}O_2$ -Based Capacitors. *Appl. Phys. Lett.* **2020**, *117* (19), 192902.

(65) Shimizu, T.; Mimura, T.; Kiguchi, T.; Shiraishi, T.; Konno, T.; Katsuya, Y.; Sakata, O.; Funakubo, H. Ferroelectricity Mediated by Ferroelastic Domain Switching in HfO_2 -Based Epitaxial Thin Films. *Appl. Phys. Lett.* **2018**, *113* (21), 212901.
(66) Lee, D. H.; Yu, G. T.; Park, J. Y.; Kim, S. H.; Yang, K.; Park, G. H.; Ryu, J. J.; Lee, J. I.; Kim, G. H.; Park, M. H. Effect of Residual Impurities on Polarization Switching Kinetics in Atomic-Layer-Deposited Ferroelectric Hf0.5Zr0.5O2 Thin Films. *Acta Mater.* **2022**, *222*, 117405.
(67) Park, J. Y.; Yang, K.; Lee, D. H.; Kim, S. H.; Lee, Y.; Reddy, P. R. S.; Jones, J. L.; Park, M. H. A Perspective on Semiconductor Devices Based on Fluorite-Structured Ferroelectrics from the Materials–Device Integration Perspective. *J. Appl. Phys.* **2020**, *128* (24), 240904.
(68) Böscke, T. S.; Govindarajan, S.; Kirsch, P. D.; Hung, P. Y.; Krug, C.; Lee, B. H.; Heitmann, J.; Schröder, U.; Pant, G.; Gnade, B. E.; Krautschneider, W. H. Stabilization of Higher-κ Tetragonal HfO2 by SiO2 Admixture Enabling Thermally Stable Metal-Insulator-Metal Capacitors. *Appl. Phys. Lett.* **2007**, *91* (7), 072902.
(69) Kim, B. S.; Hyun, S. D.; Moon, T.; Do Kim, K.; Lee, Y. H.; Park, H. W.; Lee, Y. B.; Roh, J.; Kim, B. Y.; Kim, H. H.; Park, M. H.; Hwang, C. S. A Comparative Study on the Ferroelectric Performances in Atomic Layer Deposited Hf0.5Zr0.5O2 Thin Films Using Tetrakis(Ethylmethylamino) and Tetrakis(Dimethylamino) Precursors. *Nanoscale Res. Lett.* **2020**, *15* (1), 72.
(70) Alcala, R.; Richter, C.; Materano, M.; Lomenzo, P. D.; Zhou, C.; Jones, J. L.; Mikolajick, T.; Schroeder, U. Influence of Oxygen Source on the Ferroelectric Properties of ALD Grown $Hf_{1-x}Zr_xO_2$ Films. *J. Phys. Appl. Phys.* **2021**, *54* (3), 035102.
(71) Liu, S.; Hanrahan, B. M. Effects of Growth Orientations and Epitaxial Strains on Phase Stability of HfO2 Thin Films. *Phys. Rev. Mater.* **2019**, *3* (5), 054404.
(72) Cao, R.; Wang, Y.; Zhao, S.; Yang, Y.; Zhao, X.; Wang, W.; Zhang, X.; Lv, H.; Liu, Q.; Liu, M. Effects of Capping Electrode on Ferroelectric Properties of $Hf_{0.5}Zr_{0.5}O_2$ Thin Films. *IEEE Electron Device Lett.* **2018**, *39* (8), 1207–1210. https://doi.org/10.1109/LED.2018.2846570.
(73) Lyu, J.; Song, T.; Fina, I.; Sánchez, F. High Polarization, Endurance and Retention in Sub-5 Nm $Hf_{0.5}Zr_{0.5}O_2$ Films. *Nanoscale* **2020**, *12* (20), 11280–11287.